Interfacial Tension between CO_2, Freshwater, and Brine in the Range of Pressure from (2 to 27) MPa, Temperature from (20 to 125) °C, and Water Salinity from (0 to 334 000) mg·L^{-1}

Stefan Bachu*,† and D. Brant Bennion‡

Alberta Research Council, 250 Karl Clark Road NW, Edmonton, Alberta T6N 1E4, Canada, and Hycal Energy Research Laboratories, Ltd., 1338 A, 36th Avenue NE, Calgary, Alberta T2E 6T6, Canada

An extensive laboratory program was conducted for the measurement of the interfacial tension between CO_2 and water or brine covering the ranges of (2 to 27) MPa pressure, (20 to 125) °C temperature, and (0 to 334 010) mg·L^{-1} water salinity. The laboratory experiments were conducted using the pendant drop method combined with the solution of the Laplace equation for capillarity for the profile of the brine drop in the CO_2−brine equilibrium environment. The analysis of the resulting set of 378 IFT measurements reveals that: (1) under conditions of constant temperature and water salinity, IFT steeply decreases with increasing pressure in the range $P < P_c$ and mildly decreases for $P > P_c$ with an asymptotic trend toward a constant value at higher pressures; (2) under the same conditions of constant pressure and temperature, IFT increases with increasing water salinity, reflecting decreasing CO_2 solubility in brine as salinity increases; (3) the dependence of IFT on temperature is more complex than that on either pressure or salinity, depending on the CO_2 phase. For $T < T_c$, IFT increases with increasing temperature, and around the critical point ($T \approx T_c$), IFT significantly decreases (believed to be associated with the fact that at T_c the IFT between CO_2 liquid and vapor phases tends to zero) and then increases again with increasing temperature for $T > T_c$ with an asymptotic trend toward a constant value for high temperatures. The dependence of IFT on pressure, temperature, and water salinity for CO_2 and water/brine systems can be well approximated by a power function of pressure whose coefficient and exponent depend on temperature and water salinity. These results indicate that, in the case of CO_2 storage in deep saline aquifers as a climate-change mitigation strategy, the formation water displacement by injected CO_2 during the injection (drainage) phase of CO_2 storage and the possible subsequent CO_2 displacement by invading brine during the CO_2 migration (imbibition) phase depend on in situ conditions of pressure, temperature, and water salinity through the effects that these primary variables have on the IFT between CO_2 and aquifer brine.

Introduction

The interpretation of the temperature record on a scale of centuries to millennia indicates a slight increase in global average annual temperatures in the last 150 years, and it is predicted that if the business-as-usual scenario is continued, then humankind will face significant climate change by the end of this century.[1] A major challenge in mitigating climate change effects is the reduction of CO_2 emissions in the atmosphere. Carbon dioxide capture and storage, which entails CO_2 capture from large power-generating and industrial processes, and injection into deep geological formations, plays an important role in reducing atmospheric CO_2 emissions.[2] Carbon dioxide can be sequestered in geological media through a variety of physical and geochemical mechanisms,[3] including trapping as an immobile phase in the pore space of deep saline aquifers,[4] whose water salinity usually increases with depth to values up to and greater than 400 000 mg·L^{-1} in very deep strata, in the vicinity of evaporitic beds, or both.

The processes of injection, migration, and storage of CO_2 in deep saline aquifers depend on the characteristics of brine displacement by CO_2 (drainage) during injection and at the front of a migrating CO_2 plume and of CO_2 displacement by brine (imbibition) and residual gas trapping in the wake of the migrating plume. In these displacement and CO_2 trapping cases, the relevant characteristics are the relative permeability and capillary pressure of CO_2 and the formation water systems,[5,6] which both depend on the interfacial tension (IFT) between CO_2 and formation water (brine). For the same rock and under the same conditions of pressure, temperature, and water salinity, gas relative permeability depends on IFT, with relative permeability varying in the opposite direction to IFT, as shown by experiments for CO_2/brine systems[7,8] and gas/oil/water systems[9] and by comparative displacements for CO_2/oil/brine and N_2/oil/brine systems[10] and CO_2/brine and H_2S/brine systems.[11] Therefore, through its effect on relative permeability, the IFT between CO_2 and in situ brine impacts CO_2 trapping and storage at irreducible saturation and the ability of CO_2 to flow and possibly migrate and leak out of the storage unit.

Because CO_2 storage in geological media and particularly in deep saline aquifers is a recently emerging field, until very recently, interest has been mostly focused on CO_2−oil systems because of the potential use of CO_2 for enhanced oil recovery; only limited sets of data have been published regarding the IFT between CO_2 and water, and no data on the relative permeability of CO_2−brine systems have been published. Because of the

* Corresponding author. E-mail: Stefan.Bachu@arc.ab.ca. Tel: +1-780-450-5467. Fax: +1-780-450-5083.
† Alberta Research Council.
‡ Hycal Energy Research Laboratories, Ltd.

10.1021/je800529x CCC: $40.75
Published on Web 12/31/2008

Table 1. Range of Temperature and Water Salinity for IFT Measurements[a]

	Water Salinity ($mg \cdot L^{-1}$)					
T/°C	0	75 780	144 300	225 460	282 770	334 010
20	×		×			×
25	×	×	×	×	×	×
26	×		×			×
28	×		×			×
30	×		×			×
32	×		×			×
34	×		×			×
35	×		×			×
36	×		×			×
41	×	×	×	×	×	×
60	×		×			×
75	×	×	×	×	×	×
100	×		×			×
125	×	×	×	×	×	×

[a] Notes: (1) Water salinities are characteristic of formation waters in the Wabamun Lake area in the Alberta basin; (2) Measurements were made for each set of temperature and water salinity for pressures of (2, 4, 6, 8, 12, 17.4, and 27) MPa for a total of 378 IFT measurements.

Table 2. Composition of the Brines Used in the IFT Measurements

	water salinity ($mg \cdot L^{-1}$)				
ion	75 780	144 300	225 460	282 770	334 010
sodium (Na)	24 738	40 474	63 900	74 998	94 000
potassium (K)	225	0	2100	2346	0
calcium (Ca)	3931	9948	17 100	23 420	24 400
magnesium (Mg)	455	3468	2560	4128	3750
chloride (Cl)	46 369	89 614	139 000	177 000	211 100
sulfate (SO_4)	13	265	571	669	643
bicarbonate (HCO_3)	49	535	231	207	115
total dissolved solids (TDS)	75 780	144 304	225 462	282 768	334 008

absence of data in the public domain on the displacement characteristics of CO_2−brine systems, in 2004, we started a laboratory program for the measurement of CO_2−brine relative permeability and capillary pressure under in situ conditions on sandstone, carbonate, shale, and anhydrite core samples from sedimentary strata in the Alberta basin, Canada.[11] These experiments included IFT measurements,[7,8] which is a prerequisite for measuring the displacement characteristics of CO_2−brine systems. Noticing an emerging pattern in the distribution of IFT data as measured under the specific in situ conditions of pressure, temperature, and water salinity in central Alberta,[7] we initially expanded the IFT measurement program to cover a range of salinity and supercritical temperature ($T > T_c$) systematically, with some partial results being presented only in graphical form.[12] On the basis of the clearly emerging pattern of IFT dependence on pressure, temperature, and salinity, the measurement program was subsequently expanded to cover a range of subcritical temperature ($T < T_c$) as well. The results of the full measurement program are presented here in both tabular and graphic form for the temperatures and water salinities shown in Table 1 and for pressures of (2, 4, 6, 8, 12, 17.4, and 27) MPa. Measurements were made for the full spectrum of temperatures for pure water and brines of 144 300 $mg \cdot L^{-1}$ and 334 010 $mg \cdot L^{-1}$ salinity. Measurements across the full water−salinity spectrum were made for temperatures of (25, 41, 75, and 125) °C.

Previous Work

Under normal standard conditions, CO_2 is a gas with a density of 1.872 $kg \cdot m^{-3}$. The critical point for CO_2 is $T_c = 31.04$ °C and $P_c = 7.38$ MPa, where *T* and *P* are temperature and pressure,

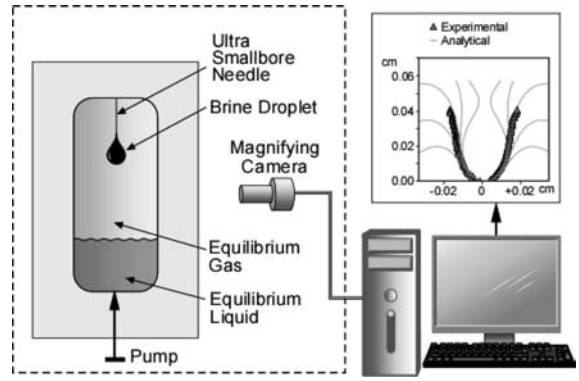

Figure 1. Schematic diagram of the apparatus used for IFT measurements.

Table 3. Experimental IFT Data for CO_2−Pure Water Systems

	P/MPa						
T/°C	2	4	6	8	12	17.4	27
20	62.4	43.5	34.9	29.1	25.1	23.2	18.9
25	62.1	45.1	36.2	30.6	26.5	24.9	21.1
26	61.8	45.6	36.5	30.8	26.9	25.0	21.3
28	62.0	46.1	37.6	32.8	27.4	25.8	22.3
30	62.1	48.2	39.7	33.5	27.7	26.4	25.7
32	62.5	49.1	40.7	34.8	28.6	27.4	26.1
34	61.5	38.2	31.5	27.3	18.5	16.4	16.1
35	62.1	39.3	31.9	27.4	18.6	16.6	16.3
36	64.9	39.6	32.1	27.5	19.0	17.3	16.6
41	65.2	42.9	33.2	28.5	19.9	17.8	16.9
60	66.6	52.9	43.1	37.9	31.2	29.4	28.8
75	66.9	53.2	43.6	38.6	34.5	31.5	29.9
100	67.7	57.9	47.5	41.7	37.6	32.9	32.1
125	68.1	58.9	50.5	44.6	39.6	36.1	33.2

respectively, and the subscript c denotes the critical point. For $T < T_c$ and pressures above the vaporization curve, CO_2 is a liquid, whereas for temperatures and pressures above the critical point, CO_2 is a supercritical fluid. The quadruple point temperature for CO_2 is 10.2 °C, below which CO_2 may form hydrates in the presence of water. In the case of CO_2 storage in geological media, in situ temperatures will generally be higher than the quadruple point and likely be higher than the critical point, but low temperatures below the critical point and possibly even below the quadruple point will likely be encountered in the case of CO_2 storage in deep marine sediments or below the permafrost in arctic regions.

The surface tension of liquid−vapor systems for pure substances displays a dependence on pressure and temperature and vanishes for the critical temperature T_c.[13] For binary CO_2−brine systems, the water phase can be regarded as nearly incompressible in the temperature and pressure ranges of interest, but the CO_2 phase is highly compressible. In addition, IFT for CO_2−water systems is affected by the low level of mutual solubility in the pressure and temperature ranges of interest.[14] The critical point of CO_2 in the presence of water is very close to the critical point of pure CO_2,[15] with the difference less than 0.5 °C such that at 32 °C (as in experiments reported here), CO_2 is supercritical. Given the dependence of CO_2 density on pressure and temperature and the dependence of CO_2 solubility in water on pressure and temperature,[16] it is expected that pressure and temperature have an effect on IFT, particularly for gaseous CO_2. Because the surface tension of aqueous electrolytes increases with increasing salinity as a result of ion hydration[17] and because of the decreasing CO_2 solubility in brine with increasing water salinity,[18] an effect of water salinity on IFT for CO_2−brine systems should also be expected.

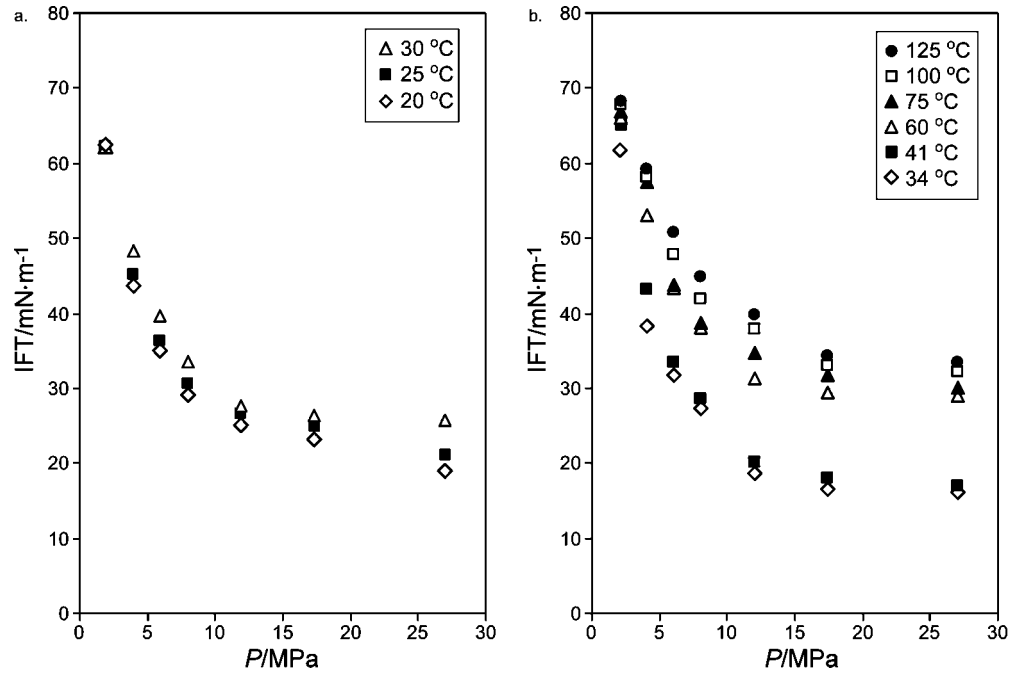

Figure 2. Variation of IFT with pressure and temperature for CO_2−pure water systems for (a) subcritical temperatures ($T < T_c$) and (b) supercritical temperatures ($T > T_c$).

Table 4. Coefficients of the Exponential Fit to IFT Isotherms for CO_2−Pure Water and CO_2−Brine of 144 300 mg·L^{-1} and 334 010 mg·L^{-1} Salinity in the Pressure Range of (2 to 27) MPa and Temperature Range of (20 to 125) °C

	salinity (mg·L^{-1})								
	0			144 300			334 010		
T/°C	A	B	R^2	A	B	R^2	A	B	R^2
20	81.102	0.4551	0.9839	84.249	0.3686	0.9802	86.573	0.2721	0.9608
25	78.819	0.4168	0.9788	84.165	0.3621	0.9783	87.568	0.2623	0.9630
26	78.744	0.4130	0.9805	83.803	0.3555	0.9771	87.617	0.2573	0.9643
28	78.717	0.3992	0.9841	84.113	0.3500	0.9818	87.817	0.2537	0.9615
30	77.034	0.3687	0.9508	83.674	0.3394	0.9821	78.828	0.2910	0.9779
32	77.910	0.3620	0.9599	82.875	0.3419	0.9831	79.129	0.3083	0.9693
34	84.024	0.5491	0.9625	80.981	0.3862	0.9516	81.622	0.3114	0.9757
35	85.373	0.5506	0.9612	82.406	0.3870	0.9541	83.192	0.3016	0.9715
36	87.406	0.5524	0.9607	83.679	0.3896	0.9571	87.394	0.3098	0.9789
41	90.959	0.5543	0.9690	86.077	0.3934	0.9642	85.778	0.2807	0.9731
60	82.198	0.3508	0.9554	83.017	0.3370	0.9798	85.059	0.2458	0.9765
75	84.422	0.3404	0.9563	83.722	0.3140	0.9774	84.186	0.2148	0.9611
100	85.697	0.3206	0.9720	86.016	0.2984	0.9588	86.495	0.2095	0.9345
125	86.236	0.3009	0.9887	88.440	0.2871	0.9412	87.806	0.1985	0.8950

Table 5. Experimental IFT Data for CO_2 and 144 300 mg·L^{-1} Brine Systems

	P/MPa						
T/°C	2	4	6	8	12	17.4	27
20	63.5	51.1	45.3	41.3	31.3	28.4	25.8
25	63.9	51.3	46.0	41.7	31.8	28.7	26.5
26	64.1	51.5	46.3	42.0	32.2	29.0	27.1
28	64.6	52.0	46.8	42.5	33.0	29.9	27.4
30	65.1	52.5	47.0	43.2	33.5	31.0	28.2
32	65.4	51.0	45.6	42.9	33.1	30.5	27.8
34	65.2	46.5	42.6	34.4	27.7	26.0	25.5
35	65.6	47.8	43.1	35.5	28.1	26.1	25.9
36	66.0	48.5	43.7	36.1	28.5	26.1	26.0
41	66.1	51.2	44.3	37.2	29.2	26.5	26.1
60	67.1	53.0	45.1	40.5	34.2	30.4	29.5
75	67.5	55.5	48.8	42.9	35.9	33.1	31.7
100	68.9	59.5	53.1	46.2	37.8	35.0	34.2
125	69.3	62.8	56.5	49.1	39.2	37.4	36.3

Table 6. Experimental IFT Data for CO_2 and 334 010 mg·L^{-1} Brine Systems

	P/MPa						
T/°C	2	4	6	8	12	17.4	27
20	68.1	64.3	55.3	47.8	42.2	38.9	36.2
25	69.8	65.5	56.8	49.3	43.8	40.5	37.9
26	69.9	65.9	57.2	50.3	44.5	41.0	38.4
28	70.1	66.5	57.8	50.8	44.9	41.6	38.9
30	62.7	55.4	47.8	42.9	36.5	33.1	31.5
32	61.4	54.8	47.3	41.8	34.2	31.9	29.8
34	62.7	56.2	48.5	43.0	36.2	32.1	30.1
35	63.1	58.9	50.2	44.9	38.6	34.0	30.8
36	66.5	60.1	52.4	46.4	39.5	35.1	31.5
41	67.4	61.4	53.5	48.6	41.2	36.8	34.9
60	67.9	62.8	56.6	52.1	46.1	42.0	36.7
75	69.3	64.4	59.5	55.8	49.9	44.7	40.1
100	69.7	65.9	62.5	58.6	53.1	46.4	41.1
125	70.5	67.8	64.5	62.4	56.0	48.6	42.5

For temperatures in the (0 to 50) °C range and pressures up to 6 MPa, the isotherms of IFT of CO_2 and pure water systems as a function of pressure are slightly convex in shape to the pressure axis for $T < T_c$, are almost linear in the vicinity of T_c, and are slightly concave in shape for $T > T_c$.[19] More detailed measurements for CO_2−pure water in the temperature range of (5 to 71) °C and pressures in the (0.1 to 20) MPa range reveal that:[20,21] (1) IFT decreases almost linearly with pressure in the

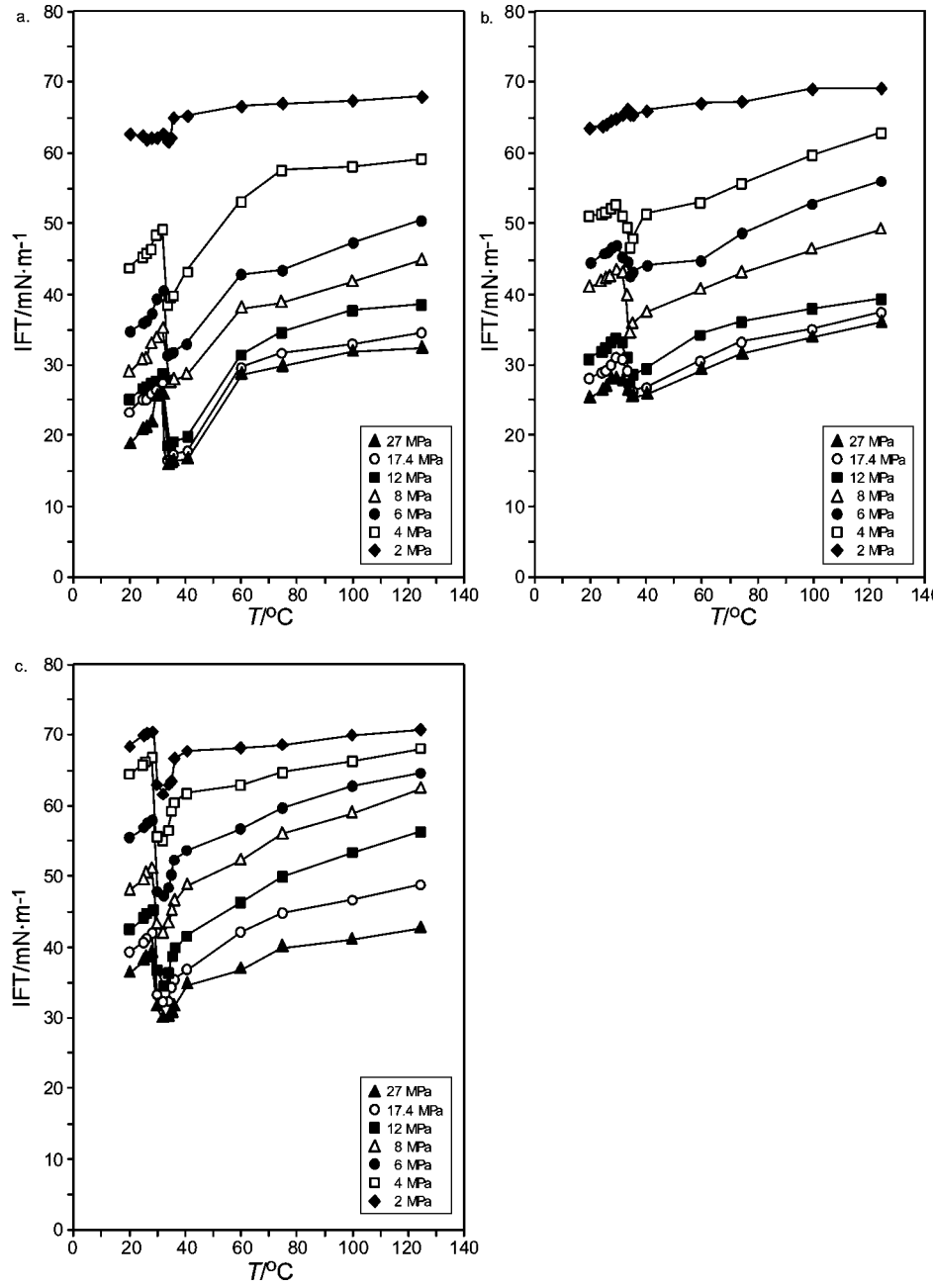

Figure 3. Variation of IFT with pressure and temperature along isobars: for (a) CO_2−pure water systems, (b) CO_2 and brine of 144 300 mg·L^{-1} salinity, and (c) CO_2 and brine of 334 010 mg·L^{-1} salinity.

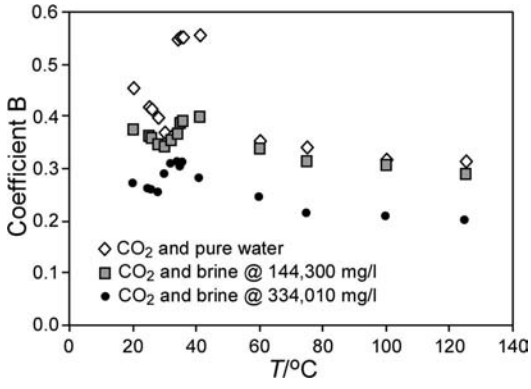

Figure 4. Variation in temperature with the values of the exponent *B* of the exponential fit to IFT isotherms.

low-pressure range (gaseous CO_2) but is largely independent of pressure at high pressure (liquid or supercritical CO_2), reaching an equilibrium value of approximately 20 mN·m^{-1}. This decrease is attributed to increasing solubility of CO_2 in water. (2) IFT isotherms cross over at pressures of about 3 MPa. IFT decreases with temperature at pressures below this and increases with temperature at pressures above it. (3) IFT isotherms for $T < T_c$ are separated into two parts that are interrupted at the CO_2 vaporization pressure. Below this pressure, the isotherm reflects the IFT between water and gaseous CO_2, which decreases almost linearly with pressure, whereas above the vaporization pressure, the isotherm represents the IFT between liquid water and liquid CO_2. For $T > T_c$, IFT isotherms continuously decrease with increasing pressure. (4) For $T < T_c$, the IFT isotherms show a dip, which was also observed previously[22,23] but not always, with the effect being strongest and at the lowest pressure for the lowest temperature (5 °C) and diminishing and shifting toward higher pressures but still less than P_c as the temperature is increased and

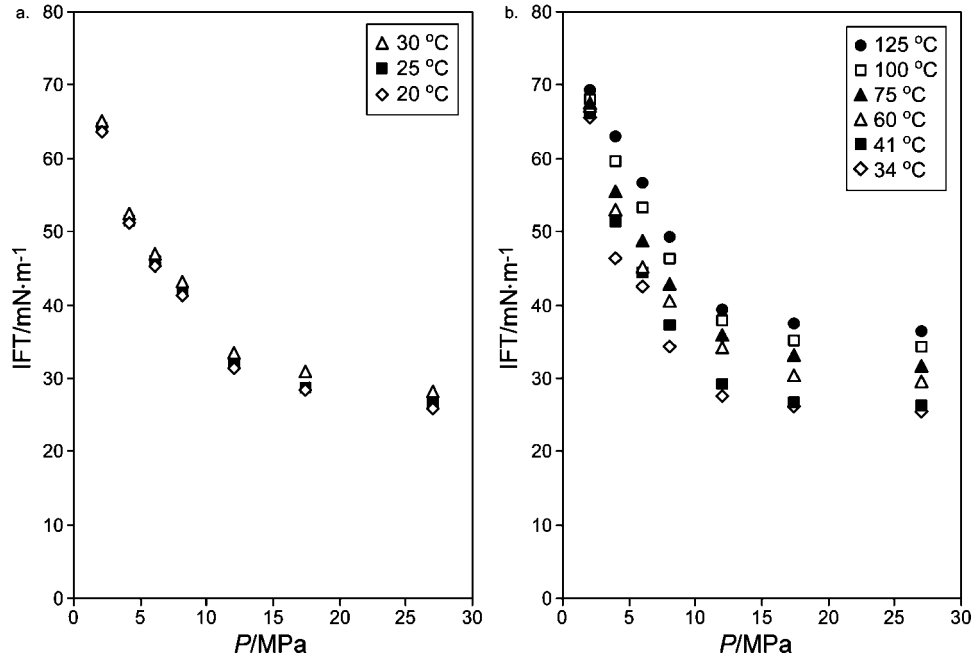

Figure 5. Variation of IFT with pressure and temperature for CO_2 and brine of 144 300 mg·L^{-1} salinity for (a) subcritical temperatures ($T < T_c$) and (b) supercritical temperatures ($T > T_c$).

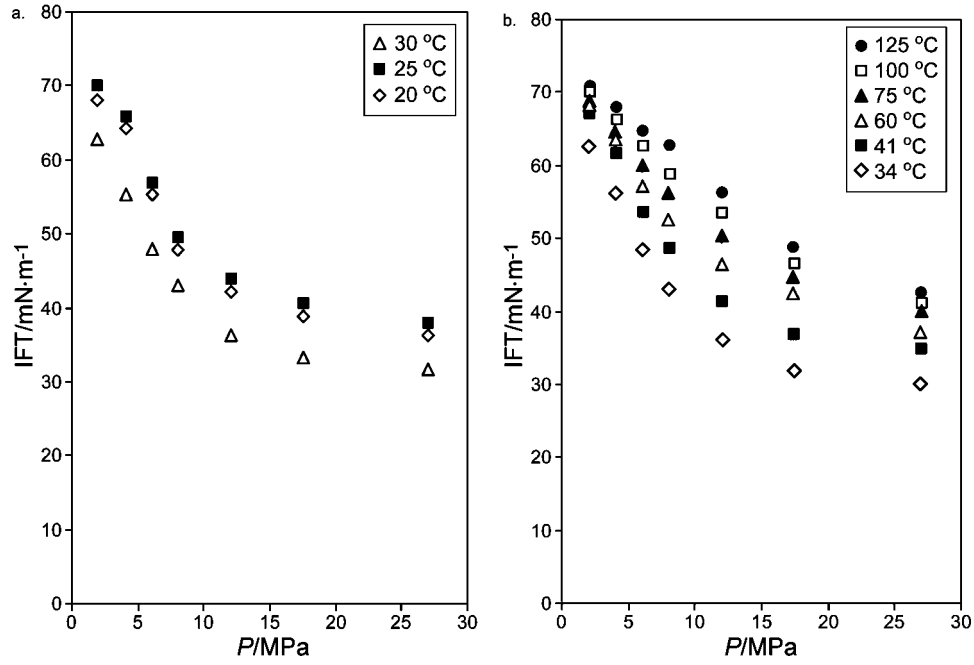

Figure 6. Variation of IFT with pressure and temperature for CO_2 and brine of 334 010 mg·L^{-1} salinity for (a) subcritical temperatures ($T < T_c$) and (b) supercritical temperatures ($T > T_c$).

Table 7. Experimental IFT Data for CO_2 and 75 780 mg·L^{-1} Brine Systems

	P/MPa						
T/°C	2	4	6	8	12	17.4	27
25	62.9	50.5	44.9	39.9	31.0	28.2	25.1
41	65.8	45.9	37.9	32.7	25.5	23.8	22.5
75	66.9	54.2	47.3	41.9	34.3	31.9	30.5
125	68.9	61.5	55.5	47.5	38.9	35.2	33.4

Table 8. Experimental IFT Data for CO_2 and 225 460 mg·L^{-1} Brine Systems

	P/MPa						
T/°C	2	4	6	8	12	17.4	27
25	69.3	63.0	54.2	47.7	42.9	39.8	37.1
41	66.3	55.2	47.9	40.4	36.6	34.0	33.4
75	68.5	59.8	54.6	46.1	42.7	37.5	34.5
125	69.8	63.6	59.0	56.7	51.2	44.1	40.1

approaches T_c. The size and "width" of the dip around the critical point varies, although this effect may be an artifact of the measurements (i.e., the different pressure intervals at which measurements were made). This dip is most likely related to the phase change of CO_2 from gaseous to liquid, where the shift in pressure at which the dip occurs roughly corresponds to the increase in the vaporization pressure as temperature increases toward T_c. (5) In the proximity of the CO_2 critical point, the IFT between pure gas and liquid-phase CO_2 becomes very small and reaches a minimum (theoretically vanishing[23]), which is

Table 9. Experimental IFT Data for CO_2 and 282 770 mg·L^{-1} Brine Systems

	P/MPa						
T/°C	2	4	6	8	12	17.4	27
25	69.5	64.2	55.2	48.2	43.5	40.2	37.5
41	66.5	59.5	49.5	47.6	40.1	35.2	34.2
75	69.1	62.0	57.0	51.1	45.1	41.3	38.9
125	69.9	64.5	60.9	59.5	52.5	45.7	41.6

explained by the appearance of a third-phase intermediate in composition between the water and CO_2-rich phases.[20]

The crossover of IFT isotherms in the (3 to 4) MPa interval that reaches a plateau at (8 to 10) MPa was observed also by Tewes and Boury,[24] who conducted IFT measurements in the pressure range of (2 to 9) MPa for temperatures of (20, 30, and 40) °C. Yang et al.[25,26] studied the IFT for CO_2−crude oil systems and CO_2−brine systems in the pressure range of (0.1 to 31.4) MPa and for temperatures of (27 and 58) °C. The salinity of the oil-field brine used in the experiments was quite low (4270 mg·L^{-1} total dissolved solids) and close to the legal definition of potable groundwater. The authors report for both temperatures a decrease in IFT as pressure increased. The increase in IFT as temperature increased is attributed to the decrease in CO_2 solubility in water/brine as temperature increased. For $T = 27$ °C $< T_c$ the IFT increased between measurements at (4 and 8.5) MPa because of the CO_2 phase change from gas to liquid.

Regarding the effect of water salinity, Cai et al.[27] reported for hydrocarbon−brine systems a weak dependence of IFT on pressure but a significant dependence of IFT on temperature and salinity. (IFT increases with increasing temperature, NaCl concentration, or both.) Chalbaud et al.[28] report IFT measurements for CO_2−brine systems in the pressure range of (4.5 to 25.5) MPa for temperatures of (27, 71, and 100) °C that correspond to liquid and supercritical CO_2 and NaCl concentrations between (0.085 and 2.56) mol·L^{-1}. They conclude that the IFT for CO_2−brine systems decreases with increasing pressure and increases with increasing temperature and salinity (as expected), but above a certain pressure, IFT reaches a plateau that is independent of temperature and pressure. For pressures below the plateau limit, the authors conclude that the increase in IFT with increasing salinity is linear, with a slope that is constant for a large range of concentrations and that depends on temperature before the constant IFT value is reached.

In a study directed at CO_2 storage rather than enhanced oil recovery, Chiquet et al.[29] presented IFT measurements in the temperature and pressure range of (35 to 110) °C and (5 to 45) MPa, respectively, for a CO_2−pure water system and along the 35 °C isotherm for a CO_2−brine system (20 000 mg·L^{-1} NaCl solution). They concluded that the presence of salt has a negligible effect on IFT and that along a given isotherm IFT sharply decreases at the beginning and then levels off and reaches a pseudoplateau for $P > 20$ MPa, a plateau that decreases slightly with temperature. In addition, the authors hypothesize that the IFT values measured in the low-pressure range (> 5 MPa nevertheless) linearly extrapolate to $P \approx 0$ to the liquid−vapor IFT of pure water, which decreases quasi-linearly from 72.74 mN·m^{-1} at 20 °C to ~ 54 mN·m^{-1} at 125 °C.[30] This hypothesis seems to be supported by previous measurements at 0.1 MPa by Chun and Wilkinson[20] and Hebach et al.[21] and at 2 MPa by Tewes and Boury.[24] However, Yang et al.[25,26] report much lower IFT values of 49.4 mN·m^{-1} for 0.121 MPa at 27 °C and of 69.45 mN·m^{-1} for 0.13 MPa at 58 °C, which is ~ 3 mN·m^{-1} greater than the liquid−vapor IFT of pure water at the same temperature.

An examination of the data previously published in graphic and tabular form by various authors[20−22,24−26,28,29] shows that measurements differ by as much as several micronewtons per meter for the same pressure and temperature. These differences can be attributed to the measurement method (pendant drop versus capillary rise), to equilibrium versus dynamic IFT (i.e., water pre-equilibrated with CO_2 or not), and to potential errors due to the method of calculating the densities of the two components (water and CO_2).

As mentioned in the Introduction, the work reported here covers a much broader range of brine salinity and temperature (both sub- and supercritical) than any previous work, with close temperature spacing in the vicinity of T_c. (See Table 1.)

Experimental Setting

The IFT measurements were conducted using the pendant drop method that was originally developed by Hauser and his colleagues[31,32] and has been employed since then by many researchers, including work previously referenced.[21,24−26,28] Distilled water was used for the CO_2−freshwater experiments. The brines were reconstructed in the laboratory on the basis of specific formation water analyses from the respective formations in central Alberta (Table 2). The waters are of the NaCl type but do contain other trace components as well, which is consistent with the composition of actual oilfield brines in Alberta.

Because it is essential that the two fluids are in thermodynamic equilibrium to avoid mass transfer[33] and obtain a stable IFT, the CO_2 and water or brine were precontacted with each other at the specific measurement temperature and pressure in a piston cell prior to each measurement and were shaken until an equilibrium condition of saturation had been established between the two phases. (The CO_2-rich phase was saturated with water vapor, and the aqueous-rich phase was saturated with CO_2.) This is essential because if the two phases are not in proper equilibrium under each set of conditions for which IFT is to be evaluated, then a stabilized drop profile will not be obtained because of mass transfer effects between the phases.[33] The two equilibrium phases were then separated; constant temperature and pressure were maintained using transfer pistons contained within the oven and pulsation-free positive displacement pumps (keeping pressure constant to within 10 kPa and temperature constant to within 0.5 °C during the transfer process), and the interface between the two phases was discarded (to avoid contamination of either pure equilibrium phase). The density of each separate phase was precisely measured using an Anton PAAR DMA 512 digital high-pressure density meter. Accurate density measurements are essential to the drop pendant method for IFT determination, and this apparatus provides precise phase density values to 0.0001 g·cm^{-3} at pressures of up to 45 MPa and temperatures of up to 150 °C on single-phase systems. Given the precision of the temperature and pressure measurements for the system (± 0.5 °C and ± 0.01 MPa), we feel that the actual precision of the density measurements is approximately ± 0.001 g·cm^{-3}. Density values are not reported in this work because of practical limitations on the size of the data set (twice the size of the IFT data set). Once the individual phase densities had been determined, the optical IFT cell was charged while constant temperature and pressure systems were maintained with the equilibrium gas phase. Figure 1 provides a schematic illustration of the apparatus.

The equilibrium brine phase, also maintained under constant temperature and pressure conditions, was gently extruded through the needle in the drop pendant apparatus to form

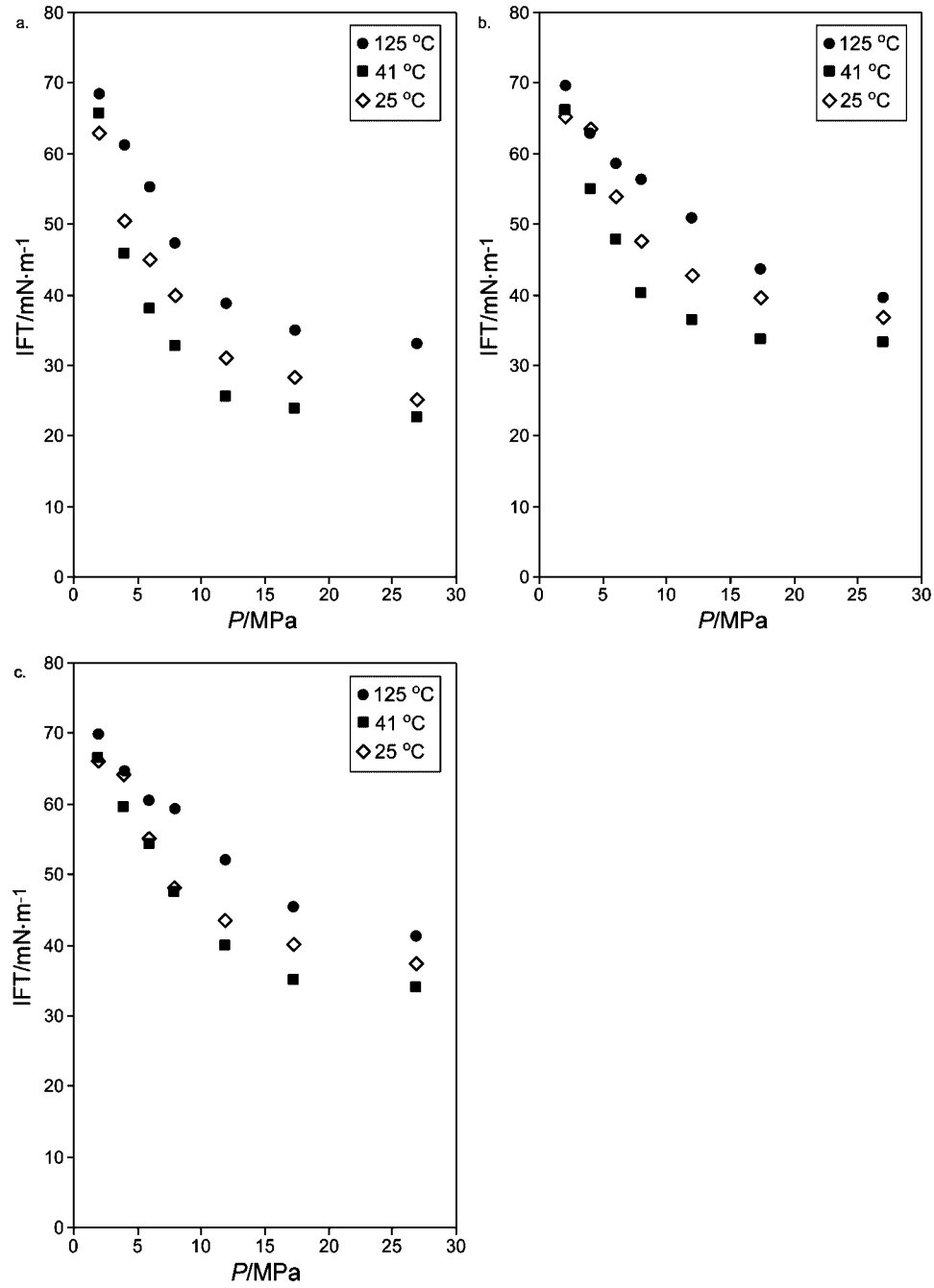

Figure 7. Variation of IFT with pressure and temperature for CO_2 and brines of various salinities: (a) 75 780 mg·L^{-1}, (b) 225 460 mg·L^{-1}, and (c) 282 770 mg·L^{-1}.

Table 10. Coefficients of the Exponential Fit to IFT Isotherms for CO_2 and Brines of 75 780 mg·L^{-1}, 225 460 mg·L^{-1}, and 282 770 mg·L^{-1} Salinity in the Pressure Range of (2 to 27) MPa and Temperature Range of (25 to 125) °C

	salinity (mg·L^{-1})								
	75 780			225 460			282 770		
T/°C	A	B	R^2	A	B	R^2	A	B	R^2
25	83.626	0.3725	0.9855	86.059	0.2650	0.9662	86.534	0.2626	0.9651
41	77.230	0.4027	0.9705	79.155	0.2873	0.9544	85.206	0.2875	0.9641
75	83.271	0.3257	0.9755	85.590	0.2796	0.9825	84.034	0.2391	0.9814
125	90.346	0.3130	0.9612	85.254	0.2188	0.9633	85.320	0.2060	0.9419

approximately 10 cm^3 of equilibrium liquid phase at the base of the measurement cell. Following an additional 24 h of further equilibration time, a pendant drop was extruded onto the tip of the needle. Previously reported experiments have shown that equilibration times on the order of hundreds of seconds are needed,[21,25,33] but experiments reported by Tewes and Boury[24] indicated that equilibrium IFT values obtained after 60 000 s (~ 16.67 h) were slightly lower than those obtained after shorter equilibration times because of continuing equilibration. The droplet of equilibrium brine, surrounded by the equilibrium gas, was then suspended under measurement temperature and pressure conditions from the tip of the needle, which was

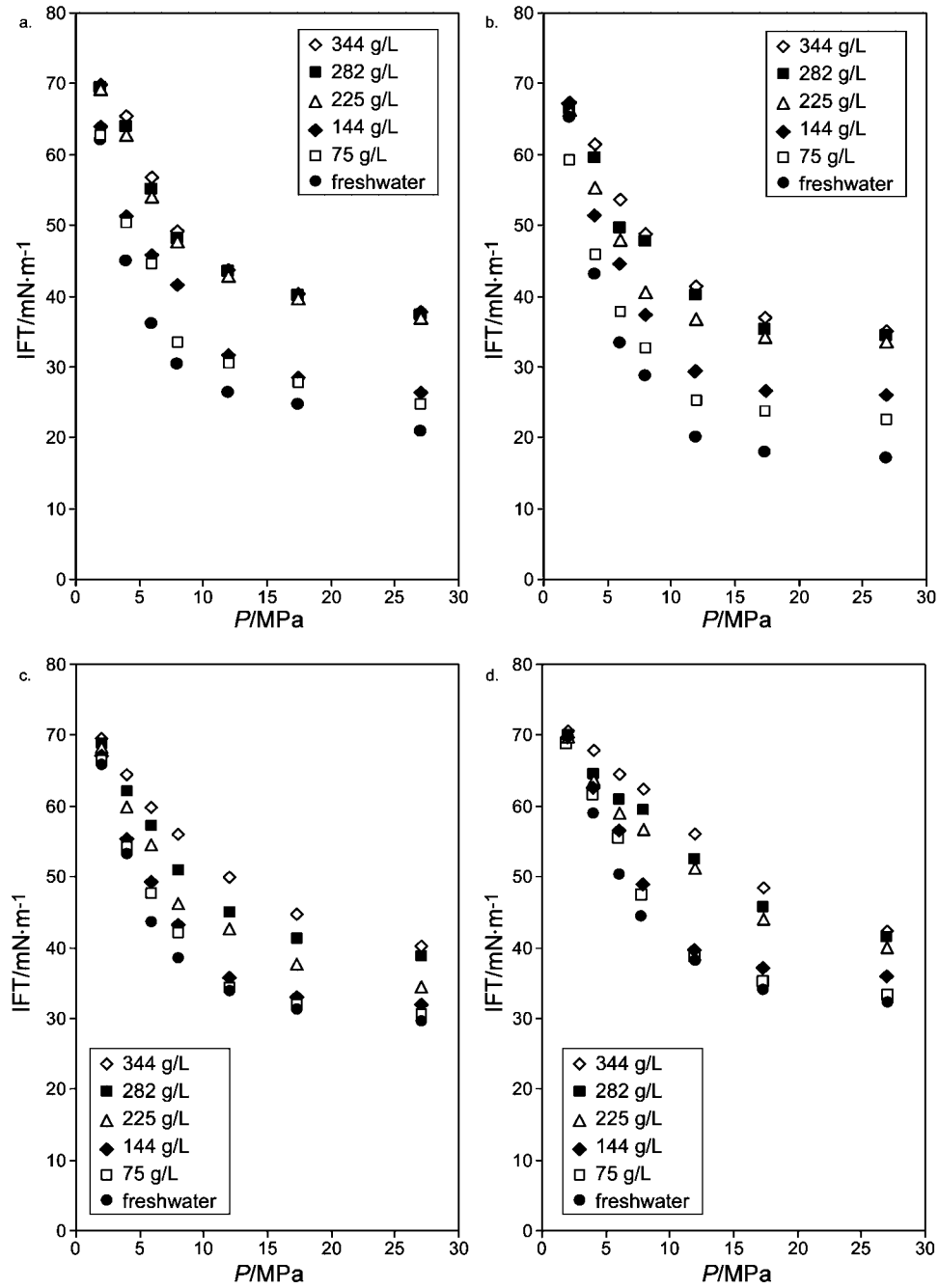

Figure 8. Variation of IFT with pressure and water salinity for CO_2 and brines at various temperatures: (a) 25 °C, (b) 41 °C, (c) 75 °C, and (d) 125 °C.

extended into the optically visible portion of the sight cell until an equilibrium configuration was obtained for at least 1 h. The inside diameter of the needle used in the tests (composed of Hastalloy C alloy) was either (0.03302 or 0.05588) mm, depending on the level of IFT to be measured. It was found that even with pre-equilibration of the fluids it was necessary to allow the 24 h pre-equilibration phase in the cells because, otherwise, stable droplet profiles were difficult to obtain. At this time, a well-focused digital high-magnification image of the configuration of this drop was obtained. The drop image was shown on a digital monitor and updated twice every second. The final equilibrium profile was digitally captured with a precision of ± 1 % by a frame-grabber program and extracted in an electronic file. An optimization software package was used to match the surface curvature of the drop with the solution of the Laplace equation for capillarity for the solution of the IFT. A detailed description of this method is provided in the literature[34,35] and in some of the papers previously referenced.[24,29]

Errors and uncertainties in results can be caused by errors and uncertainties in pressure, temperature, and density measurements and in the capture of the drop image and its use in the inverse Laplace equation to determine IFT values. IFT calculations depend on the density difference between the two fluids, and uncertainties, σ, in IFT introduced by pressure, temperature, and density uncertainties would normally be assessed using the law of propagation of errors

$$\sigma_{\mathrm{IFT}}^2 = \sigma_{\rho \mathrm{H_2O}}^2 + \sigma_{\rho \mathrm{CO_2}}^2 \quad (1)$$

where the uncertainty in density itself can be estimated from the uncertainty in pressure, P, and temperature, T, according to

$$\sigma_\rho^2 = \left(\frac{\partial \rho}{\partial P}\right)^2 \sigma_P^2 + \left(\frac{\partial \rho}{\partial T}\right)^2 \sigma_T^2 \quad (2)$$

Of the two, temperature has a greater effect than pressure on the density of both CO_2 and brine. The uncertainties in water density measurements are quite low given water's almost incompressible character and small coefficient of thermal expansion, such that the uncertainty in temperature and pressure introduced by measurement accuracy leads to an uncertainty of less than 0.01 % in water or brine density over the range of temperature and pressure that is under consideration. However, CO_2 is much more compressible, and its density is much more sensitive to temperature, particularly in the vicinity of the critical point, where pressure and temperature variations in the range of measurement precision (0.5 °C and 0.01 MPa) may have a significant effect on density. The experimental data in this data set cannot be used for estimating uncertainties because of the large difference in the data set in pressure and temperature around the critical point (ΔP = 2 MPa and ΔT = 2 °C). Although CO_2 and water or brine densities were directly measured with a precision of ± 0.001 g·cm^{-3}, to provide an estimate of the order of magnitude in uncertainties and on the basis of the fact that the density of the water-saturated CO_2 phase is extremely close to that of pure CO_2,[29] the density of CO_2 was calculated using the equation of state developed by Span and Wagner[36] for P and T values in the (6 to 8) MPa and (32 to 34) °C interval varying in increments equal to the measurement precision. Calculations using these data indicate that close to the CO_2 critical point the measurement precision for temperature in particular can introduce uncertainties in the corresponding difference in phase densities of approximately 5 %, whereas the uncertainty introduced by the precision in pressure measurements is lower by slightly more than 2 orders of magnitude. This would translate to a precision of approximately ± 2 mN·m^{-1} for the calculated values of IFT under conditions close to the CO_2 critical point. For regions farther away from the critical point, the variations in CO_2 density are much smaller, and hence the measurement precision is expected to be in the range of ± 0.5 mN·m^{-1} and less, as found in previous work.[21,29] However, the uncertainty in IFT values measured under pressure and temperature conditions close to the critical point does not diminish the value of the data, particularly in light of the consistency in trends, as will be seen below.

Results

It should be noted here that in this set of measurements, CO_2 is in the supercritical phase for all measurements for which $T \geq 32$ °C and $P \geq 8$ MPa. For measurements at $T < 32$ °C, CO_2 is in the liquid phase for $T = 20$ °C and $P \geq 6$ MPa and for $P \geq 8$ MPa for all of the other measurements, otherwise CO_2 is in the gaseous phase. The phase change and sharp increase in CO_2 density across the vaporization curve is reflected in the results.

Interfacial Tension for CO_2−Water Systems. The results of IFT measurements for CO_2−pure water systems are presented in Table 3 and shown graphically in Figure 2. The data display the pattern noted in previous work of decreasing IFT with increasing pressure along isotherms, with a steep decrease at the beginning, followed by a very slow decrease for pressures that are generally greater than the critical pressure, P_c. Some isotherm cross-over is also present around 3 MPa, as previously noted. However, no dip in IFT isotherms for $T < T_c$ is observed, as previously identified.[20−23] The most probable reason for not observing the dip in the IFT isotherms is that measurements at ΔP = 2 MPa intervals are insufficient for capturing the dip and that measurements at pressures much closer to the vaporization pressure and to P_c are needed.[20,21] Whereas one may argue that the IFTs are all reaching a plateau with an asymptotic tendency toward a single value,[28] the data clearly show that whereas each isotherm tends to level off, they remain distinct. Furthermore, the data show that IFT increases with increasing temperature for $T < T_c$, drops around T_c, and then resumes its increase with increasing temperature for $T > T_c$ (Figure 2), which is best illustrated in Figure 3a, where the variation of IFT with temperature is shown along isobars. This dip in IFT likely corresponds to the vanishing of IFT for $T = T_c$ for pure CO_2 systems.[23] Although not identified and discussed by the authors, the same pattern of IFT variation with temperature along isobars is evident in the IFT data for water−CO_2 systems reported by Chun and Wilkinson.[20]

For the range of pressure and temperature used in these experiments, the IFT isotherms for CO_2−pure water systems can be described by an empirical exponential equation of the form

$$\mathrm{IFT} = \mathrm{A} \cdot P^{-\mathrm{B}} \quad (3)$$

Table 4 shows the coefficient, A, and exponent, B, for each IFT isotherm and the R^2 of the fit. Whereas this relationship has no physical basis, it can be used, nevertheless, to estimate IFT values for other sets of pressure, temperature, and water salinity for which no direct measurements are available. An examination of the variation in the values of the exponent B (Table 4 and Figure 4) clearly indicates the existence of two regimes, each broadly corresponding to $T < T_c$ and $T > T_c$.

The results obtained for CO_2−pure water systems were compared, where possible, with previously published data. (No comparison could be made for CO_2−brine systems because no such measurements have been performed to date for the range of high water salinity evaluated in this work.) A very good match was obtained between the IFT values measured in this study and previously published data for temperatures of (25 and 60) °C. However, the results at 35 °C, the only other temperature value for which IFT was measured both by others and in this study, are consistently lower than those of previously published data. The IFT data for 35 °C measured in this study are, nevertheless, consistent with the measured data for (34 and 36) °C (Table 3) and with the data measured at the same temperatures for higher salinities (next section). Considering the sensitivity of IFT determination to the density difference between CO_2 and pure water, we attribute this discrepancy to the potential large variation in CO_2 density around the critical point and to possible small differences in measuring CO_2 density between this work and previous work. It is also known that near the critical temperature for pure CO_2, the IFT between the dense and less-dense CO_2 tends to zero. Our data would appear to suggest that this trend is also reflected in the CO_2-saturated-water−water-saturated-CO_2 equilibrium situation near the critical temperature, just as some other authors have observed near the critical pressure levels.

Interfacial Tension for CO_2−Brine Systems. Tables 5 and 6 present the IFT data for CO_2 and brines of 144 300 mg·L^{-1} and 334 010 mg·L^{-1} salinity, respectively, for the same temperatures and pressures as those for CO_2−pure water systems. Figures 5 and 3b show the IFT isotherms and isobars, respectively, for CO_2 and the 144 300 mg·L^{-1} brine, and Figures 6 and 3c show the same for the 334 010 mg·L^{-1} brine. The features of IFT variation with pressure and temperature in these cases are identical to those for CO_2 and pure water, with two differences: (1) The IFT for CO_2−brine systems is greater than

the IFT for pure water for the same pressure and temperature, resulting in an upward shift in the IFT isotherms and isobars that increases with increasing salinity; and (2) the variations in isotherms and isobars is milder (smaller slope and in a narrower range) in the case of the CO_2−brine systems than in the case of the CO_2−pure water systems. This is reflected in the values and variation of the exponent B of the power fit to the IFT isotherms (Table 4 and Figure 4), the latter also being milder and varying in a narrower range. The upward shift translates to values of the exponent B that decrease with increasing water salinity for the same isotherm (Table 4).

Tables 7, 8, and 9 and Figure 7 present IFT isotherms for CO_2 and brines with salinities of 75 780 mg·L^{-1}, 225 460 mg·L^{-1}, and 282 770 mg·L^{-1}, respectively, for which measurements were made for fewer temperatures (Table 1). The IFT isotherms generally display the same characteristics as those for pure water and the 144 300 mg·L^{-1} and 334 010 mg·L^{-1} brines, with the IFT for $T = 41$ °C > T_c being less than the IFT for $T = 25$ °C < T_c. Some of the isotherms show a tendency for an inflection point at low pressures, corresponding to the possibility of a cross-over around 3 MPa. Although there are less data for these cases, they suggest the same pattern of increasing IFT with increasing temperature for $T < T_c$, followed by a dip around T_c, and then again a continuous increase for $T > T_c$. Another feature apparent from these IFT isotherms is the continuous shift upward in IFT as salinity increases and a relative flattening of the isotherms, with milder slopes for both low and high pressures. These isotherms can be expressed by the same exponential fit as that for pure water and the 144 340 mg·L^{-1} and 334 010 mg·L^{-1} brines, with ever decreasing exponents as salinity increases indicating a shift upward in the IFT iso-salinity curves of variation with pressure for the regimes below and above the critical temperature T_c (Table 10). The increase in IFT with increasing salinity and the upward shift of the isotherms are best illustrated in Figure 8. The results clearly show a continuous and strong dependence of the IFT for CO_2 and pure water or brine systems on pressure, temperature, and water salinity. Previous conclusions that differences between IFT values for CO_2−pure water and CO_2−brine systems are below experimental uncertainty (estimated to be in the range of ± 1 mN·m^{-1}) and that IFTs for CO_2−brine systems are very close to those of pure water under similar pressure and temperature conditions[29,37] were reached for very diluted brines (20 000 mg·L^{-1} and 0.5 M) compared with the range of brines used in this study. This dependence of the IFT for CO_2 and water or brine systems on pressure, temperature, and salinity for the ranges of P, T, and salinity, S, of the experiments presented in this article could be expressed in a generalized form as

$$\mathrm{IFT} = A(T, S) \cdot P^{-B(T,S)} \tag{3a}$$

although no attempt was made to find the functional forms of A and B.

The effects of pressure, temperature, and salinity on IFT are due to both CO_2 solubility and phase effects. The IFT between CO_2 and water or brine is different for subcritical CO_2 and supercritical CO_2, as previously identified for a smaller range of pressure and temperature.[20,21] As CO_2 solubility increases with increasing pressure and decreases with increasing temperature and water salinity, it affects the IFT, which directionally changes in the opposite direction (i.e., decreases with decreasing pressure and increases with increasing temperature and water salinity) within each of the subcritical and supercritical regions. A break in this trend is observed around the critical point for CO_2. For temperatures between (41 and 125) °C and salinities of (0, 144 300, and 334 010) mg·L^{-1}, this relationship between CO_2 solubility in water and brine and IFT for CO_2 and water or brine systems was expressed in a polynomial form[38] through regression fitting of the IFT data measured in this experimental program and corresponding CO_2 solubility values calculated under the same conditions of pressure, temperature, and water salinity using literature algorithms.[39]

Conclusions

An extensive laboratory program was conducted for the measurement of the IFT between CO_2 and water or brine covering a wide range of pressure, temperature, and brine salinity characteristic of deep saline aquifers in sedimentary basins where CO_2 may be sequestered as a climate change mitigation strategy. The laboratory experiments were conducted using the pendant drop method combined with the solution of the Laplace equation for capillarity for the profile of the brine drop in the CO_2-rich environment. The analysis of the extensive set of 378 IFT measurements revealed that: (1) Under conditions of constant temperature and water salinity, IFT steeply decreases with increasing pressure in the range $P < P_c$ and mildly decreases for $P > P_c$ with an asymptotic trend toward a plateau value for high pressures. (2) Under the same conditions of constant pressure and temperature, IFT increases with increasing water salinity, reflecting decreasing CO_2 solubility in brine as salinity increases, regardless of CO_2 phase. (3) The dependence of IFT on temperature is more complex than that on either pressure or salinity, being basically a function of CO_2 phase. For $T < T_c$, IFT increases with increasing temperature, reflecting decreasing CO_2 solubility in water or brine. Around the critical point ($T \approx T_c$), IFT significantly decreases, which is believed to be due to the theoretically zero IFT between liquid and vapor phase CO_2 under these conditions, and then increases again with increasing temperature for $T > T_c$, with an asymptotic trend toward a constant value for high temperatures. We do not expect zero IFT for $T = T_c$ because both equilibrium phases under consideration are mixtures of water and CO_2. A previously observed dip in IFT isotherms around the CO_2 vaporization point and P_c was not captured most likely because of the large pressure interval ($\Delta P = 2$ MPa) of the series of experiments reported here. (4) For the ranges of pressure, temperature, and water salinity of these experiments, the dependence of IFT on these three primary variables for CO_2 and water/brine systems can be well approximated by an empirical power function of pressure, whose coefficient and exponent depend on temperature and water salinity.

The results reported here and previously indicate that the formation water displacement by injected CO_2 during the injection (drainage) phase of CO_2 storage in deep saline aquifers and the CO_2 displacement by invading brine during the CO_2 migration (imbibition) phase depend on the in situ conditions of pressure, temperature, and water salinity through the effects that these primary variables have on the IFT between CO_2 and aquifer brine, which in turn affects capillary pressure and relative permeability. The results reported here are important because (1) of the intrinsic value of the IFT measurements, particularly for CO_2−brine systems, (2) they reveal trends and dependencies of IFT on the in situ conditions of pressure, temperature, and water salinity, and (3) they indicate the existence of two different regimes, one for subcritical CO_2 and one for supercritical CO_2. Empirical expressions fitting the data set are provided for estimating IFT values for cases under conditions of pressure, temperature, and water salinity that are different than those

measured and reported here, even if in some cases the estimated values will not necessarily be as precise as those measured in the laboratory.

Literature Cited

(1) IPCC (Intergovernmental Panel on Climate Change). *Climate Change 2007: The Physical Science Basis*, Fourth Assessment Report; IPCC Secretariat: Geneva, Switzerland, 2007.

(2) IEA (International Energy Agency). *Prospects for CO_2 Capture and Storage*; IEA/OECD: Paris, France, 2004.

(3) *IPCC Special Report on Carbon Dioxide Capture and Storage*; Metz, B., Davidson, O., de Coninck, H. C., Loos, M., Mayer, L. A., Eds.; Cambridge University Press for the Intergovernmental Panel on Climate Change: Cambridge, U.K., 2005.

(4) Kumar, A.; Ozah, R.; Noh, M. H.; Pope, G. A.; Bryant, S. L.; Sepehrnoori, K.; Lake, L. W. Reservoir Simulation of CO_2 Storage in Deep Saline Aquifers. *SPE J.* **2005**, *10*, 336–348.

(5) Bryant, S. L.; Lakshminarasimhan, S.; Pope, G. A. Buoyancy-Dominated Multiphase Flow and Its Impact on Geological Sequestration. Proceedings of the SPE/DOE Symposium on Improved Oil Recovery, Tulsa, OK, April 2−26, 2006; SPE Paper 99938.

(6) Juanes, R.; Spiteri, E. J.; Orr, F. M., Jr.; Blunt, M. Impact of Relative Permeability Hysteresis on Geological CO_2 Storage. *Water Resour. Res.* **2006**, *42*, W12418, doi:10.1029/2005WR004806.

(7) Bennion, D. B.; Bachu, S. The Impact of Interfacial Tension and Pore Size Distribution/Capillary Pressure Character on CO_2 Relative Permeability at Reservoir Conditions in CO_2−Brine Systems. Proceedings of the SPE/DOE Symposium on Improved Oil Recovery, Tulsa, OK, April 22−26, 2006; SPE Paper 99325.

(8) Bennion, D. B.; Bachu, S. Dependence on Temperature, Pressure and Salinity of the IFT and Relative Permeability Displacement Characteristics of CO_2 Injected in Deep Saline Aquifers. Proceedings of the SPE Annual Technical Conference and Exhibition, San Antonio, TX, Sept 24−27, 2006; SPE Paper 102138.

(9) Cinar, Y.; Marquez, S.; Orr, F. M., Jr. Effect of IFT Variation and Wettability on Three-Phase Relative Permeability. *SPE Reservoir Eval. Eng.* **2007**, *10*, 211–220.

(10) Dria, D. E.; Pope, G. A.; Sepehrnoori, K. Three-Phase Gas/Oil/Brine Relative Permeabilities Measured under CO_2 Flooding Conditions. *SPE Reservoir Eng.* **1993**, *8*, 143–150.

(11) Bennion, D. B. Bachu, S. Drainage and Imbibition Relative Permeability Relationships for Supercritical CO_2/Brine and H_2S/Brine Systems in Intergranular Sandstone, Carbonate, Shale and Anhydrite Rocks. *SPE Reservoir Eval. Eng.* **2008**, *11*, 487–496: doi: 19.2118/99326PA.

(12) Bachu, S. Bennion, D. B. Effects of in Situ Conditions on Relative Permeability Characteristics of CO_2−Brine Systems. *Environ. Geol.* **2008**, *54*, 1707–1722: doi: 10.1007/s00254-007-0946-9.

(13) Navascués, G. Liquid Surfaces: Theory of Surface Tension. *Rep. Prog. Phys.* **1979**, *42*, 1131–1186.

(14) King, M. B.; Mubarak, A.; Kim, J. D.; Bott, T. R. The Mutual Solubilities of Water with Supercritical and Liquid Carbon Dioxide. *J. Supercrit. Fluids* **1992**, *5*, 296–302.

(15) Morrison, G. Effects of Water upon the Critical Point of Carbon Dioxide and CO_2. *J. Phys. Chem.* **1981**, *85*, 759–761.

(16) Kohl, A. L.; Nielsen, R. B. *Gas Purification*; Gulf Publishing: Houston, TX, 1997.

(17) Levin, Y.; Flores-Mena, J. E. Surface Tension of Strong Electrolytes. *Europhys. Lett.* **2001**, *56*, 187–192.

(18) Enick, R. M.; Klara, S. M. CO_2 Solubility in Water and Brine under Reservoir Conditions. *Chem. Eng. Commun.* **1990**, *90*, 23–33.

(19) Jho, C.; Nealon, D.; Shogbola, S.; King, A. D., Jr. Effect of Pressure on the Surface Tension of Water: Adsorption of Hydrocarbon Gases and Carbon Dioxide on Water at Temperatures between 0° and 50°C. *J. Colloid Interface Sci.* **1978**, *65*, 141–154.

(20) Chun, B.-S.; Wilkinson, G. T. Interfacial Tension in High-Pressure Carbon Dioxide Mixtures. *Ind. Eng. Chem. Res.* **1995**, *34*, 4371–4377.

(21) Hebach, A.; Oberhof, A.; Dahmen, N.; Kögel, A.; Ederer, H.; Dinjus, E. Interfacial Tension at Elevated Pressures−Measurements and Correlations in the Water + Carbon Dioxide System. *J. Chem. Eng. Data* **2002**, *47*, 1540–1546.

(22) Hough, E. W.; Heuer, G. J.; Walker, J. W. An Improved Pendant Drop, Interfacial Tension Apparatus and Data for Carbon Dioxide and Water. *Pet. Trans. AIME* **1959**, *216*, 469–472.

(23) Wielebinski, D.; Findenegg, G. H. Measurement of Interfacial Tension in Simple Two-Phase Systems along an Isothermal Linear Path to the Critical Point. *J. Phys. Chem.* **1984**, *88*, 4397–4401.

(24) Tewes, F.; Boury, F. Thermodynamic and Dynamic Interfacial Properties of Binary Carbon Dioxide−Water System. *J. Phys. Chem.* **2004**, *108*, 2405–2412.

(25) Yang, D.; Tontiwachwuthikul, P.; Gu, Y. Interfacial Tensions of the Crude Oil + Reservoir Brine + CO_2 Systems at Pressures up to 31 MPa and Temperatures of 27°C and 58°C. *J. Chem. Eng. Data* **2005**, *50*, 1242–1249.

(26) Yang, D.; Tontiwachwuthikul, P.; Gu, Y. Interfacial Interactions between Reservoir Brine and CO_2 at High Pressures and Elevated Temperatures. *Energy Fuels* **2005**, *19*, 216–223.

(27) Cai, B.-Y.; Yang, J.-T.; Guo, T.-M. Interfacial Tension of Hydrocarbon + Water/Brine Systems under High Pressure. *J. Chem. Eng. Data* **1996**, *41*, 493–496.

(28) Chalbaud, C.; Robin, M.; Egermann, P. Interfacial Tension of Brine/CO_2 Systems at Reservoirs Conditions. In *8th International Conference on Greenhouse Gas Control Technologies*, Trondheim, Norway, June 19−22, 2006 [CD-ROM]; Gale, J., Rokke, N., Zweigel, P., Swenson, H., Eds.; Elsevier: Oxford, U.K., 2006.

(29) Chiquet, P.; Daridon, J.-L.; Broseta, D.; Thibeau, S. CO_2/Water Interfacial Tensions under Pressure and Temperature Conditions of CO_2 Geological Storage. *Energy Convers. Manage.* **2007**, *48*, 736–744.

(30) IAPWS Release on Surface Tension of Ordinary Water Substance, 1994. International Association for the Properties of Water and Steam Web site. http://www.iapws.org/relguide/surf.pdf.

(31) Andreas, J. M.; Hauser, E. A.; Tucker, W. B. Boundary Tension by Pendant Drops. *J. Phys. Chem.* **1938**, *42*, 1001–1019.

(32) Hauser, E. A.; Michaels, A. S. Interfacial Tension at Elevated Pressure and Temperature I. *J. Phys. Chem.* **1948**, *52*, 1157–1165.

(33) Hebach, A; Martin, G.; Kögel, A.; Dahmen, N. Interfacial Tension during Mass Transfer of CO_2 into Water in a Water-Saturated CO_2 Atmosphere at 298 K and 6.6 MPa. *J. Chem. Eng. Data* **2005**, *50*, 403–411.

(34) Cheng, P.; Li, D.; Boruvka, L.; Rotenberg, Y.; Neumann, A. W. Automation of Axisymmetric Drop Shape Analysis for Measurement of Interfacial Tensions and Contact Angles. *Colloids Surf.* **1990**, *93*, 151–167.

(35) del Rio, O. I.; Neumann, A. W. Axisymmetric Drop Shape Analysis: Computational Methods for the Measurement of Interfacial Properties from the Shape and Dimensions of Pendant and Sessile Drops. *J. Colloidal Interface Sci.* **1997**, *196*, 136–147.

(36) Span, P.; Wagner, W. Equation of State for Carbon Dioxide Covering the Fluid Region from the Triple Point Temperature to 1,100 K at Pressures up to 800 MPa. *J. Chem. Ref. Data* **1996**, *25*, 1509–1596.

(37) Massoudi, R.; King, A. D., Jr. Effect of Pressure on the Surface Tension of Aqueous Solutions, Adsorption of Hydrocarbon Gases, Carbon Dioxide and Nitrous Oxide on Aqueous Solutions of Sodium Chloride and Tetran-butyl Ammonium Bromide at 25 °C. *J. Phys. Chem.* **1975**, *79*, 1670–1675.

(38) Bennion, D. B.; Bachu, S. A Correlation of the Interfacial Tension between Supercritical-Phase CO_2 and Equilibrium Brines as a Function of Salinity, Temperature and Pressure. Proceedings of the SPE Annual Technical Conference and Exhibition, Denver, CO, Sept 21−24, 2008; SPE Paper 114479.

(39) Duan, Z.; Sun, R.; Zhu, C.; Chou, I. An Improved Model for the Calculation of CO_2 Solubility in Aqueous Solutions Containing Na^+, K^+, Ca^{2+}, Cl^- and SO_4^{2-}. *Mar. Chem.* **2005**, *98*, 131–139.

Received for review July 8, 2008. Accepted November 29, 2008.

JE800529X